



Published in final edited form as:

ACS Chem Biol. 2021 August 20; 16(8): 1526–1537. doi:10.1021/acscchembio.1c00396.

Combined Effect of Anti-SSEA4 and Anti-Globo H Antibodies on Breast Cancer Cells

Ruey-Herng Lee^{1,2}, Yu-Jen Wang^{1,3}, Ting-Yen Lai¹, Tsui-Ling Hsu¹, Po-Kai Chuang⁴, Han-Chung Wu⁵, Chi-Huey Wong^{1,4,*}

¹Genomics Research Center, Academia Sinica, Taipei, Taiwan 115

²Department of Chemistry, National Taiwan University, Taipei, Taiwan 106

³Institute of Biochemical Sciences, National Taiwan University, Taipei, Taiwan 106

⁴Department of Chemistry, The Scripps Research Institute, La Jolla, CA 92037

⁵Institute of Cellular and Organismic Biology, Academia Sinica, Taipei, Taiwan 115

Abstract

The globo-series glycosphingolipids (SSEA3, SSEA4, and Globo H) were shown to express in many cancers selectively and a combination of anti-SSEA4 and anti-Globo H antibodies was able to suppress tumor growth in mice inoculated with breast cancer cell lines. To further understand the effect, we focused on the combined effect of the two antibodies in target binding and antibody dependent cellular cytotoxicity (ADCC) *in vitro*. Here, we report that the binding of anti-Globo H antibody (VK9) to MDA-MB231 breast cancer cells was influenced by anti-SSEA4 antibody (MC813–70), and combination of both antibodies induced similar effect as did anti-SSEA4 antibodies alone in reporter-based ADCC assay, indicating that SSEA4 is a major target in breast cancer due to its higher expression than Globo H. Furthermore, we have shown that a homogeneous anti-SSEA4 antibody (chMC813–70-SCT) designed to maximize the ADCC activity can be used to isolate a subpopulation of NK cells which exhibit around 23% increase in killing the target cells as compared to the unseparated NK cells. These findings can be used to predict therapy outcome based on the expression levels of antigens and evaluate therapeutic antibody development.

*Corresponding Author: Chi-Huey Wong, Genomics Research Center, Academia Sinica, 128 Academia Rd., Sec 2, Taipei, Taiwan 115 and Department of Chemistry, The Scripps Research Center, 10550 N. Torrey Pines Rd., La Jolla, CA 92037 USA. wong@scripps.edu.;

Other co-authors:

Ruey-Herng Lee, Department of Chemistry, National Taiwan University, Taipei, Taiwan 106 and Genomics Research Center, Academia Sinica, 128 Academia Rd., Sec 2, Taipei, Taiwan 115. Current address: Tanvex Biologics Corporation, 33F., No.99, Sec. 1, Xintai 5th Rd., Xizhi Dist., New Taipei City 221, Taiwan.

Yu-Jen Wang, Institute of Biochemical Sciences, National Taiwan University, Taipei, Taiwan 106. Genomics Research Center, Academia Sinica, 128 Academia Rd., Sec 2, Taipei, Taiwan 115.

Ting-Yen Lai, Genomics Research Center, Academia Sinica, 128 Academia Rd., Sec 2, Taipei, Taiwan 115.

Tsui-Ling Hsu, Genomics Research Center, Academia Sinica, 128 Academia Rd., Sec 2, Taipei, Taiwan 115.

Po-Kai Chuang, Department of Chemistry, The Scripps Research Institute, 10550 N. Torrey Pines Rd., La Jolla, CA 92037

Han-Chung Wu, Institute of Cellular and Organismic Biology, Academia Sinica, 128 Academia Rd., Sec 2, Taipei, Taiwan 115.

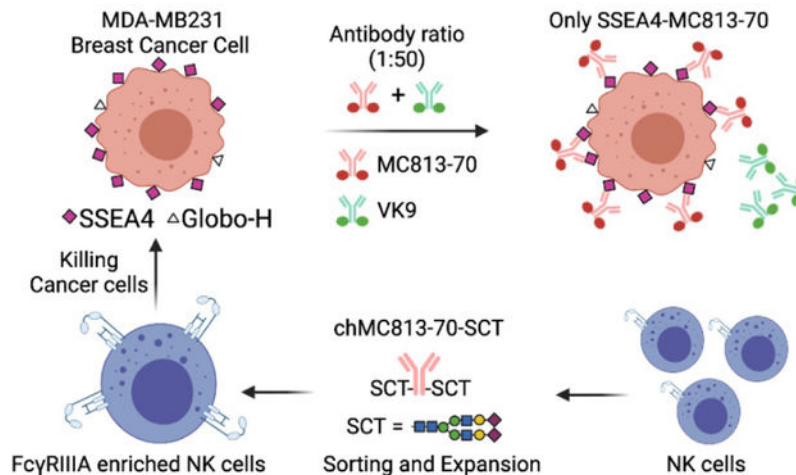
Supporting Information

The supporting information is available free of charge at <https://pubs.acs.org/doi/10.1021/acscchembio.1c00396>

Scatter plots for Figure 3 and raw data for Figure 6, Figure 7.

The authors declare no competing financial interest.

Graphical Abstract



Keywords

SSEA4; Globo H; ADCC; Isolation of NK cells

Introduction

Carbohydrates are often linked to lipids and proteins through glycosylation and expressed on cell surface. They are involved in protein folding and many cellular recognition events.¹⁻³ However, the roles carbohydrates play in biology have not been well understood until recently more advanced technology and more in-depth research have been reported, and their importance in biological processes has now been brought to light 1.

Glycosphingolipids (GSLs) are the major glycolipids in the plasma membranes that consist of a glycan attached to a lipid moiety called ceramide. Variations in glycan and ceramide structures produce a tremendous diversity of GSLs which are further classified into several series, such as ganglio, lacto, globo, etc2. GSL synthesis is initiated in the endoplasmic reticulum (ER) in which a sphingolipid base is condensed with an acyl-CoA to form a ceramide which can be transported by ceramide transfer proteins (CERTs) to trans-Golgi network (TGN) for the synthesis of sphingomyelin, or by vesicular transport to cis-Golgi to generate glucosylceramide (GlcCer). GlcCer can then be transported either by another lipid transfer protein, four-phosphate adaptor protein 2 (FAPP2) or by vesicular transport to the luminal leaflet of TGN where GlcCer is galactosylated to form lactosylceramide (LacCer) which is further glycosylated with various glycosyltransferases in TGN to give different GSL series. Though GSL expression is not template driven, different cell types tend to exhibit specific GSL expression. In fact, GSL expression is strictly regulated during development and can serve as cell-type-specific marker3. It was found that LacCer synthase (LCS) preferentially interacts with GM3 synthase (GM3S) in the Golgi cisternae, while it interacts with Gb3 synthase (Gb3S) in the TGN. If LacCer is transported via vesicular transport to the Golgi cisternae, it is primarily converted to ganglio-series GSLs. On the

other hand, if LacCer is transported by FAPP2 to the TGN, it is converted to globo-series GSLs⁴.

GSLs tend to form cluster in the lipid raft of the cell membrane and participate in various biological activities, including cell adhesion, proliferation, signaling, immune response, and infection. One study showed that the interaction between ganglioside GM3s can facilitate adhesion and spreading of mouse melanoma B16 cell line⁵. Another study showed that GSLs can have opposite effect: the ganglioside GD3 and globo-series Gb3 can inhibit proliferation in normal breast cell line MCF10A by activating Merlin/NF2 tumor suppressor gene⁶. The fatty acid component of ceramide was found responsible for GSL signaling, and the metabolite sphingosine-1-phosphate could induce immune response⁷. LacCer, can enhance neutrophils' phagocytosis of microorganisms⁸, but many studies have shown that it is a target for some pathogens to infect cells⁹. As more and more biological functions of GSLs are uncovered, it is not surprising that GSL deregulation plays a role in human diseases. Indeed, the aberrant GSL expression has been observed in many neurological diseases as well as cancers. Overexpression of ganglioside GM1 in Alzheimer's disease was found to accelerate β -sheet formation of amyloide- β proteins^{10–12}. In Parkinson's disease, however, GM1 expression is much reduced¹³. Mice with Huntington's disease had increased expression of GD1a and reduced expression of GM2-Neu¹⁴. Ganglioside GD2 is overexpressed in a wide range of cancers and can activate signaling associated with proliferation, invasion, and motility. So far several anti-GD2 antibodies have been approved for clinical use¹⁵. More evidence has shown that ganglioside GD3 is a new potential target due to its ability to mediate tumor growth and high expression in many cancers¹⁶. Overall, the various biological functions of GSLs and their wide expression in human diseases have made GSLs a promising target in immunotherapy.

Globo-series GSLs

Globo-series GSLs contain the basic structure globotriaose (Gb3), or Gal α 1,4Gal β 1,4GlcCer. Addition of a β -linked N-acetylgalactosamine (GalNAc) to the terminal galactose of Gb3 generates globotetraose (Gb4). Galactosylation of Gb4 catalyzed by β 1,3-galactosyltransferase V (β 3GalT5) produces stage-specific embryonic antigen 3 (SSEA3), which serves as the precursor of SSEA4 and Globo H. Fucosylation of terminal galactose of SSEA3 by fucosyltransferase-1 (FUT-1) and fucosyltransferase-2 (FUT-2) forms Globo H¹⁷, while sialylation of terminal galactose of SSEA3 by β -galactoside α 2,3-sialyltransferase (ST3Gal-II) forms SSEA4 (Figure 1). SSEA3 and SSEA4 were originally observed on the pluripotent cells of the inner cell mass of a blastocyst during early embryonic development, but were lost upon differentiation. Therefore, scientists have used them to isolate human embryonal stem cells (hESCs). Other studies also showed that SSEA4 is expressed in stem cells from kidneys, testes, and ovaries^{18–20}. Although SSEA4 expression in normal cells is rare, it was found to increase rapidly in many cancers, including breast cancers²¹, basaloid lung cancer²², osteosarcoma²³, prostate cancer²⁴, ovarian cancer²⁵, and oral cancer²⁶. In addition, the anti-SSEA4 antibody MC813–70 was found to be able to trigger CDC in GBM cell lines expressing SSEA4 *in vitro* and inhibit the growth of a GBM cell line in a xenograft mouse model²⁷. In addition to its broad expression in cancers, other studies have associated SSEA4 with characteristics of tumors,

such as tumorigenicity, metastasis, and chemoresistance. SSEA4⁺ osteosarcoma cells had higher probability to form tumors in mice than SSEA4⁻ cells²³. SSEA4⁺ prostate cancers downregulated epithelial-cell associated markers and upregulated mesenchymal markers, suggesting a gain of a migratory phenotype²⁷. High SSEA4 expression was observed in chemotherapy-resistant breast cancer cells and was correlated with poor prognosis²⁸.

In 1997, Globo H was found expressed in various epithelial cancers by immunohistochemistry, including small cell lung, breast, prostate, pancreas, gastric, ovarian, and endometrial cancers. Also, because most breast cancer specimens have Globo H expression Globo H expressed by normal cells is extremely rare and inaccessible to the immune system, it has been considered as a promising target for immunotherapy and diagnosis^{17, 29, 30}. Carbohydrates alone generally exhibit poor immunogenicity, so they are often conjugated with a carrier protein to induce better immune response. It was shown that when Globo H is conjugated to KLH and adjuvanted with QS21 (a mixture of saponins) induced a strong immune response to Globo H positive cancer cells. The vaccine was further developed by OBI for the treatment of triple-negative breast cancer and a global phase 3 clinical trials is ongoing (NCT03562637)³¹. It was also demonstrated that high IgG titers can be induced in mice when Globo H or SSEA4 is conjugated with Diphtheria toxoid (DT) and used as a vaccine in combination with an α -galactosylceramide analog (C34) designed to act as adjuvant and to induce a class switch from IgM to IgG²¹.

Previously, we found that SSEA3, SSEA4, and Globo H are overexpressed in glioblastoma multiforme (GBM) and various cancer cell lines of additional thirteen cancer types³², and SSEA3 and β 3GalT5 are specific markers for breast cancer stem cells³³. We also found that SSEA3, SSEA4, and Globo H form a complex in the lipid raft with caveolin-1 (CAV1) and focal adhesion kinase (FAK) for signaling³⁴. Since SSEA4 and Globo H are expressed in most cancers, we hypothesized that targeting SSEA4 and Globo H simultaneously may be a better strategy. Preliminary data have shown that combination using these two antibodies induced additive or synergistic tumor suppression in mice³⁴. Therefore, we would like to evaluate the combined effect of these two antibodies through ADCC assay to understand whether the effect observed *in vivo* could be reproduced in cell-based assays. Furthermore, by correlating the surface glycan staining with antibodies and their ADCC response, we can explore their use as a companion test to predict therapy outcome based on patients' expression levels of globo-series GSLs as well as to evaluate strategies for therapeutic antibody development.

Results

Surface staining of globo-series GSLs

To understand the combined effect of anti-SSEA4 and anti-Globo H antibodies, it is essential to first understand whether they influence each other when binding to their antigens. Here we used certain concentrations of direct conjugated mouse antibodies, MC813-70 (anti-SSEA4) and VK9 (anti-Globo H), to perform single staining (with one type of antibody) and double staining (with two types of antibodies) on MCF-7 and MDA-MB-231. We hypothesize that if the two antibodies do not influence each other in antigen binding, signals (mean fluorescence intensities relative to isotype control) from

single staining and double staining should be similar. On the other hand, if they influence each other, signals from single staining and double staining should be different. For single staining, cells were incubated with 10 $\mu\text{g/mL}$ MC813–70-AF488 or 5 $\mu\text{g/mL}$ VK9-APC, both of which are oversaturated concentrations much greater than their K_D values (MC813–70: 4.21 ± 0.26 nM; VK9: 1 ± 0.116 nM)^{30, 32}. For double staining, cells were incubated with antibody mixture containing MC813–70-AF488 (10 $\mu\text{g/mL}$) and VK9-APC (5 $\mu\text{g/mL}$). After flow cytometry analysis, we found that, for MC813–70, the single staining signal was comparable to double staining signal on both cell lines, indicating that VK9 does not affect antigen binding of MC813–70. For VK9, however, signals between single staining and double staining were different: MCF-7 had lower signal in double staining, whereas MDA-MB-231 had higher signal in double staining (hereinafter we referred to the difference as VK9 signal difference). This suggests that MC813–70 can affect antigen binding of VK9 (Figure 3a, Figure S1). This result prompted us to examine whether the VK9 signal difference also occurs in the double staining of SSEA3 and Globo H. Therefore, we double stained the two cell lines with MC631 (anti-SSEA3) and VK9. After three independent experiments, no significant VK9 signal difference was observed on both cell lines (Figure 3b), indicating that MC631 and VK9 do not influence each other in binding antigens.

Since mouse IgG3 antibodies have very low affinities to human Fc γ RIIIa receptor and thus induce poor ADCC response, we obtained the chimeric antibodies chAb6 (anti-SSEA4 antibodies) and chVK9 (anti-Globo H antibodies) with human IgG1 Fc portion, from Dr. HC Wu's laboratory, for the purpose of examining the ADCC response targeting SSEA4 and Globo H. First, we examined the combined effect of conjugated chAb6 and chVK9 by surface staining as well. The results showed that, similar to double staining of SSEA4 and Globo H using mouse antibodies, chAb6 signals between single staining and double staining were similar. However, interestingly, chVK9 signals between single staining and double staining were also similar (Figure 3c). This indicates that chAb6 and chVK9 do not affect each other in antigen binding. We next used these two chimeric antibodies for subsequent ADCC assay.

It is noteworthy that staining signals using conjugated antibodies are influenced by factors such as fluorophore brightness and voltage setting on flow cytometers, and thus do not reflect the actual or relative amounts of SSEA4 and Globo H. By surface staining with unconjugated chimeric antibodies (indirect method) in the following experiments, the relative amount of SSEA4 and Globo H on MCF-7 is roughly 10:1 (Figure 6, Table S3).

ChAb6 induced higher ADCC response than chVK9

To determine the ADCC response targeting SSEA4 and Globo H, we used chAb6 and chVK9 which share the same human IgG1 Fc sequence with high affinity to human Fc γ RIIIa. Before evaluating combined effect, we first tested these two antibodies separately on MCF-7, which has high levels of SSEA4 and Globo H expression among breast cancer cell lines. To measure ADCC response, here we used ADCC reporter bioassay, which has lower variability and higher accuracy and precision than PMBC-based ADCC. The results showed that chAb6 induced more significant ADCC response than chVK9, indicating SSEA4 is probably a better target than Globo H in breast cancer. This difference in ADCC

response was correlated with the difference in staining signal (by indirect method) (Figure 4, Table S1).

To further understand the difference in ADCC response, we checked Fc glycosylation of these two antibodies, which could also affect ADCC response. To this end, we digested the two antibodies with trypsin and subjected them to mass spectrometry for glycoform analysis. The results showed that both antibodies have similar N-glycan compositions, with about 80% core-fucosylation and 42% with terminal galactosylation (Table 1). Compared with other glycan structures, FA2 and FA1 showed relatively different percentages between the two antibodies. However, these two glycan structures have not been reported to affect ADCC response. We also noted that high mannose type N-glycans, which could reduce Fc core-fucosylation and thus increase ADCC, are slightly different: chAb6 (7.93%) showed somewhat higher percentage than chVK9 (4.79%). Overall, we concluded that Fc glycosylation of these two antibodies may not contribute significantly to the ADCC response difference.

ChVK9 induced little ADCC response

We then evaluated the combined effect of chAb6 and chVK9 by ADCC assay in several breast cancer cell lines that were shown to express both SSEA4 and Globo H32. In combination groups, half the amount of each antibody was added so that the total amount of antibody is equal to that in single antibody groups. After six hours of incubation with target cells and effector cells, the results showed that the combination groups induced slightly lower ADCC response than chAb6 groups for each cell line (Figure 5 main graphs, Table S2). However, when we changed the x-axis from total antibody concentration to chAb6 concentration, the combination groups and chAb6 groups almost completely overlapped (Figure 5 inset graphs). This indicates that the ADCC response induced in the combination groups is primarily from chAb6. In other words, chVK9 hardly induced ADCC response in combination. This phenomenon is particularly evident in Globo H⁺ cell lines, MCF-7 and MDA-MB-157, in which chVK9 alone did induce ADCC but did not induce higher response in the combination groups.

Positive correlation between surface expression and ADCC

For anti-SSEA4 and anti-Globo H antibodies to become therapeutic drugs, it is imperative to understand what specific groups of patients can benefit from this therapy. That is, how the expression levels of SSEA4 and Globo H are required to induce significant ADCC response. Therefore, we correlated the staining signal with the ADCC response for each antibody concentration in each breast cancer cell line to create dot plots of SSEA4 and Globo H. Here we used the same batches of chAb6 and chVK9 for surface staining and ADCC assay to establish a better correlation. In surface staining, cells were first stained with these two antibodies, followed by second incubation with AF488-conjugated goat anti-human IgG antibodies (described in Methods). The results showed that SSEA4 dot plot exhibited a fitted curve, whereas Globo H dot plot exhibited a fitted line (Figure 6, Table S3). In SSEA4 dot plot, interestingly, MCF-7 and MDA-MB-231 exhibited slightly different correlations: For each antibody concentration, MCF-7 had higher SSEA4 staining signal than MDA-MB-231, but it induced lower ADCC response than MDA-MB-231. Next when we compared the two

dot plots at the same scale, we found that for each unit increase in staining signal, chAb6 induced ADCC response more effectively than chVK9. Moreover, we noticed that, at 30 $\mu\text{g}/\text{mL}$ chVK9, the staining signals were reduced, but ADCC responses remained increasing for MCF-7 and MDA-MB-157 (Figure 6).

We further study the competition between MC813–70 and VK9 by immunostaining. The cell staining analysis showed that even MCF-7 cells, which have high expression of Globo H, are predominantly bound with MC813–70 at the 1:50 ratio between MC813–70 and VK9 (Figure 7a). This is consistent with the surface staining results (Figure 3a). To further evaluate the therapeutic potential of anti-SSEA4 antibodies, we turned the commercially available and widely used anti-SSEA4 antibody MC813–70 into a homogeneous chimeric glycoform with 2,6-sialyl complex-type glycan attached to Asn-297 (chMC813–70-SCT, Figure 7b). Based on SPR analysis and other structural studies, it was shown to enhance the avidity toward $\text{Fc}\gamma\text{III A}$ receptor and the corresponding ADCC effector function (Figure 7c)³⁵. This homogeneous antibody was then used to isolate a subpopulation of NK cells expressing $\text{Fc}\gamma\text{III A}$, and as expected the isolated NK cells showed around 23% increase in killing the target cells (MDA-MB-231) as compared to the unseparated NK cells (Figure 7d). This result reconfirms that an antibody such as MC813–70 with high avidity and specificity toward SSEA4 can be further transformed to a chimeric version to maximize its effector functions such as ADCC against target cells with high expression of SSEA4 as demonstrated in this proof of concept study.

Discussion

Though the combination of both antibodies induced better effect in mice, we did not observe the effect in ADCC cell-based assay. One possibility is that the ADCC assay we used measures effector cell activation, which does not directly reflect cell death in mice. It is also possible that the better effect observed in mice resulted from a combination of multiple effects by other possible mechanisms, such as signaling or CDC or collective effects through targeting different individual cancer cells.

Since chAb6 and chVK9 have the same Fc region, similar glycoforms, and similar affinities to their antigens, the remarkable difference in ADCC induction between chAb6 and chVK9 is due to their difference in staining signals. Surface staining of MCF-7 using unconjugated antibodies showed that, at the same antibody concentration, chAb6 signal is approximately ten times higher than chVK9 signal. Moreover, more than 95% of cell population was labeled SSEA4⁺ using 0.3 $\mu\text{g}/\text{mL}$ chAb6, whereas chVK9 could only label as high as 80% of cell population as Globo H⁺, indicating that chAb6 stains cells more effectively than chVK9. There have been many reports that showed strong correlation between antigen expression level and ADCC activity^{36, 37}. Therefore, we believe that SSEA4 is a better target than Globo H for therapeutic development due to its higher expression. Furthermore, a report showed that Siglec-7 and -9 ligands, sialic acid-containing carbohydrates, can inhibit a subpopulation of NK cells that bear Siglec-7 and -9 receptors 38. If SSEA4, which also contains sialic acids, interacts with Siglec-7 and -9 receptors to suppress NK cell activities, anti-SSEA4 antibodies could block the interaction in addition to ADCC induction. However, in the glycan array analysis, SSEA4 did not interact with Siglec-7 or Siglec-9.

The VK9 signal difference observed in the double staining of SSEA4 and Globo H using MC813–70 and VK9 is likely due to steric hindrance. As noted in several studies, steric hindrance can occur when antigens are closely spaced or when antibodies are conjugated to high molecular weight labels, such as ferritin (750 kDa) and phycoerythrin (250 kDa)^{39, 40}. Here we demonstrated that allophycocyanin (APC) (105 kDa) does not lead to steric hindrance because it, when conjugated to chVK9, did not significantly result in chVK9 signal difference in the double staining of SSEA4 and Globo H using chAb6 and chVK9 (Figure 3c). Therefore, we suspected that SSEA4 is not only more expressed than Globo H, but also is in close proximity to Globo H. This is further supported by Chuang *et al.* that globo-series GSLs formed a complex with CAV1 and FAK in the lipid raft to maintain breast cancer cell survival³⁴. Furthermore, we found that MC813–70 and chAb6 have different staining patterns in MCF-7 and MDA-MB-231 (Figures 3a and 3c), and both antibodies as well as VK9 have similar avidity to their antigens with Kd in the nanomolar range, suggesting that chAb6 and MC813–70 may bind to SSEA4 differently.

Cross-linking of Fc receptors is a critical step in triggering effector cell activation. It occurs when antibodies bind to antigens, in soluble form or on cancer cell surface, to form immune complexes, which then bring Fc receptors together to induce signaling in immune cells⁴¹. For example, Fc γ RIIIa cross-linking can induce intracellular calcium mobilization and trigger degranulation in NK cells^{42, 43}. In addition to antigen expression level, we suspected that antigen distribution may affect the level of Fc γ RIIIa cross-linking. The observation that anti-SSEA4 antibody is more effective at inducing ADCC than anti-Globo H antibody, is probably due to the higher density of SSEA4 that enhances the Fc γ RIIIa cross-linking. Also, slightly different correlations of MCF-7 and MDA-MB-231 in SSEA4 dot plot (Figure 6) and staining signal differences between SSEA4 and Globo H suggest that distributions and densities of SSEA4 and Globo H on cell surfaces between different breast cancer cell lines are different. Apart from antigen expression level and distributions, characterizing the avidity of chAb6 and chVK9 antibodies to antigens and Fc γ RIIIa can help further understand ADCC response and different correlation on each cell line.

In the correlation experiment, when chVK9 concentration reaches 30 μ g/mL, we observed a reduced staining signal but significantly higher ADCC response in MCF-7 and MDA-MB-157. We speculate that high antibody concentration might result in antibody aggregation, in which the Fc region of the antibody can still bind to Fc γ RIIIa (CD16a), while the Fab region is not bound to antigens. Fc γ RIIIa is a low affinity Fc receptor that has been reported to be able to bind aggregated IgGs and increase ADCC response^{44, 45}. However, if antibodies are aggregated due to oxidation or other reactions that destabilize their structures, ADCC response will significantly decrease^{46, 47}.

In our study, we found that expression levels of SSEA4 and Globo H were heterogeneous in various breast cancer cell lines. Thus, examining the expression levels of these two antigens on breast cancer cells is necessary to determine effectiveness of SSEA4- and Globo H-targeted therapy for patients. Apart from the correlation data (Figure 6), circulating tumor cells (CTCs) could also be examined for therapy assessment. CTCs are cells that shed from the primary tumor and enter the circulatory system, which enable them to form a new tumor in a distant tissue. Recent studies have demonstrated that CTCs contribute to breast cancer

metastasis and are indicative of worse survival in breast cancer patients^{48, 49}. They can even provide quiescent population of the tumor that could be the cause of treatment resistance. One such example is that CTCs from human epidermal growth factor receptor 2 (HER2)-negative⁻ patients were found to be HER2-positive⁵⁰. Thanks to technology advancement, breast CTCs now can be detected with high efficiency and purity^{51, 52}. Overall, we can stain patients' CTCs to examine expression levels of SSEA4 and Globo H and determine whether they are eligible for the targeted therapy or vaccination.

In conclusion, our results suggested that SSEA4 is a better target than Globo H in breast cancer due to its higher expression, and that antigen distribution and density may play a role in ADCC induction. The establishment of the correlation between staining signal and ADCC response can help assess therapy effectiveness for patients and evaluate strategies for therapeutic antibody development.

Methods

Cell culture.

Breast cancer cell lines were obtained from ATCC. MCF-7 was maintained in RPMI 1640 supplemented with 10% (vol/vol) FBS and 1X NEAA. MDA-MB-231 and T-47D were maintained in DMEM supplemented with 10% (vol/vol) FBS. MDA-MB-361 was maintained in DMEM/ F12 with 10% FBS. Other breast cancer cell lines were cultured according to American Type Culture Collection (ATCC). FBS supplemented with 5% DMSO was used as freeze medium in cryopreservation.

Production of chimeric VK9 antibodies.

Chimeric VK9 plasmids were obtained from Dr. HC Wu (ICOB, Academia Sinica). Plasmid transformation was performed using HIT DH5 α , followed by plasmid extraction (QIAGEN plasmid MEGA kit). Expi293F expression system (Thermo Fisher Scientific) was used to express chimeric VK9. Antibody purification was performed on ÄKTA start (GE Healthcare Life Sciences) using HiTrap Protein A HP column (1ml, GE Healthcare Life Sciences), followed by desalting using two HiTrap Desalting columns (5ml, GE Healthcare Life Sciences) in series to exchange buffer to 1X PBS.

For plasmid transformation, 500 ng light chain or heavy chain plasmids was incubated with 100 μ l HIT DH5 α on ice for 10 min. 10 μ l of the mixture containing plasmids and HIT DH5 α along with 100 μ l LB broth, was plated onto a prewarmed LB agar plate containing 100 μ g/mL ampicillin. Plating beads were used to spread the mixture across the plate surface, and the plate was then incubated in the incubator at 37 °C. For plasmid extraction, after centrifugation at 6000 \times g for 15 min at 4 °C, bacterial cell pellets were sequentially treated with resuspension buffer, lysis buffer, and neutralization buffer to extract plasmid DNAs, which were then purified using anion-exchange resin column. After precipitation, washed, and air-dried, plasmid DNAs were dissolved in TE buffer and stored at 4 °C.

After transfection, the transfection supernatant was first centrifuged at 8000 rpm for 15 min at 4 °C and filtered through 0.22 μ m filter. HiTrap Protein A HP column and HiTrap Desalting columns were washed with deionized water and 1X PBS before use. For antibody

purification, HiTrap Protein A HP column was equilibrated with 2 mL 1X PBS for 30 sec. During sample loading, the supernatant passed through the column at 4 mL/min for 2 hr 10 min, followed by wash with 20 mL 1X PBS. The bound chVK9 was then eluted with pH 3 glycine and neutralized with pH 9 1M Tris/HCl. (Tris/HCl:glycine ratio = 1:15). The eluents containing chVK9 were combined and subjected to desalting. Two HiTrap Desalting columns were equilibrated with 5 mL 1XPBS for 1 min. During sample loading, flow rate was set to 1 mL/min, and 5 ml 1X PBS was used to elute chVK9 for 5 min.

Antibody glycoform analysis by in-solution tryptic digestion.

First, 7.5 μ L digestion buffer (50 mM ammonium bicarbonate) and 0.75 μ L 100 mM reducing buffer (100 mM Dithiothreitol) were added to 10 μ L (2 μ g) antibody sample. The mixture was adjusted to 18.5 μ L with ultrapure water and incubated at 95°C for 5 min. Next, 1.5 μ L alkylation buffer (100 mM iodoacetamide) was added to the sample and allowed to react in the dark at room temperature for 20 min. After alkylation, the sample was treated with 1 μ L trypsin (0.4 μ g/ μ L), and was placed in the incubator at 37°C overnight. After 12–16 hours, the sample was heated to 95°C for 10 min and subjected to mass spectrometry.

For glycoform analysis, the signal for each glycan structure was normalized to percentage of the total signals. Glycan structures were further organized based on the presence of fucoses or galactoses to determine percentages of core-fucosylation and terminal galactosylation.

Surface staining and flow cytometry.

(a) Staining with direct conjugated mouse antibodies. In single staining, 0.5 μ g Alexa Fluor 488 (AF488)-conjugated anti-SSEA4 mAb (MC813–70), 0.5 μ g Alexa Fluor 488 (AF488)-conjugated anti-SSEA3 mAb (MC631), or 0.25 μ g Allophycocyanin (APC)-conjugated anti-Globo H mAb (VK9) was used to stain 2×10^5 cells in 50 μ L FACS buffer (1X PBS with 1% FBS) for 30 min at 4°C in the dark. In double staining, 0.5 μ g AF488-conjugated MC813–70 or 0.5 μ g AF488-conjugated MC631 was mixed with 0.25 μ g APC-conjugated VK9 prior to staining 2×10^5 cells. (b) Staining with direct conjugated chimeric antibodies. In single staining, 0.5 μ g Fluorescein isothiocyanate (FITC)-conjugated anti-SSEA4 chimeric mAb (chAb6) or 0.5 μ g allophycocyanin (APC)-conjugated anti-Globo H chimeric mAb (chVK9) was used to stain 2×10^5 cells in 50 μ L FACS buffer for 30 min at 4 °C in the dark. In double staining, 0.5 μ g FITC-conjugated chAb6 was mixed with 0.5 μ g APC-conjugated chVK9 prior to staining 2×10^5 cells. After 30-min incubation at 4°C in the dark, cells were washed twice with 200 μ L FACS buffer and then were re-suspended with 200 μ L FACS buffer containing 1 μ g/mL propidium iodide (PI) before flow cytometry analysis. Data acquisition was performed using FACSCanto (BD Biosciences), and data were analyzed by FlowJo (BD Biosciences). (c) Staining with unconjugated chimeric antibodies (indirect method). Cells (2×10^5) were incubated with five concentrations of unconjugated chAb6 or chVK9 (30, 10, 3.33, 1.11, 0.37 μ g/mL) in 50 μ L FACS buffer for 30 min. After primary incubation, cells were washed with 150 μ L FACS buffer and centrifuged at $500 \times g$ for 3 min to discard supernatants. For secondary incubation, cells were incubated with 50 μ L FACS buffer containing 1 μ g/mL Alexa Fluor 488 (AF488)-conjugated goat anti-human IgG antibodies for 30 min at 4 °C in the dark before flow cytometry analysis. Data acquisition

was performed using FACSCanto (BD Biosciences), and data were analyzed by FlowJo (BD Biosciences).

ADCC reporter bioassay.

ADCC reporter bioassay (Promega G7014) was performed using engineered Jurkat cells expressing human Fc γ RIIIa-V158 receptor. Multiple cross-linking of target cells with Jurkat cells by antibodies leads to Jurkat cell luciferase production, which can be quantified to determine Jurkat cell activation. Target cells were seeded at 12,500 cells per well in a 96-well white plate and incubated at 37°C, 5% CO₂ overnight. After 12–16 hours, serial dilutions of antibodies were first added to target cells; 75,000 Jurkat cells were then added to the wells already containing target cells and antibodies. The effector cell : target cell (E:T) ratio was 6:1. After 6-hour incubation at 37°C, 5% CO₂, the plate was allowed to cool to room temperature for 15 min, followed by addition of luciferase substrate. Five minutes after luciferase substrate addition, luminescence was measured using CLARIOstar (BMG Labtech). Fold of induction was calculated by dividing RLU (induced – background) by RLU (no antibody control – background). GraphPad Prism 6 software was used for data analysis.

Immunofluorescence microscopy.

Cells were seeded in 96-well plates, cultured for one day and rinsed with PBS followed by fixation with 4% paraformaldehyde/PBS at RT for 30 min and PBS rinse. After blocking with 5% BSA/PBS for 30 min, FICT-conjugated VK9 and APC-conjugated MC813–70 antibodies were added in either 1:1 (0.5 μ g/mL : 0.5 μ g/mL) or 1:50 ratio (0.5 μ g/mL : 25 μ g/mL) for double staining, or FICT-conjugated VK9 alone (0.5 or 25 μ g/mL) for single staining. Nuclei of cells were stained with Hoechst 33342 (10 μ g/mL) for 10 min followed by PBS rinse. Stained cells were mounted by 50% glycerol/PBS and subjected to Opera PhenixTM for image acquisition.

Primary human NK cell culture and ex vivo expansion of isolated NK cells.

Cryopreserved primary human NK cells were purchased from Cellero. The homogeneous antibody chMC813–70-SCT with 2,6-sialyl complex-type glycan (SCT) attached to Asn-297 prepared according to the procedure described previously⁵⁰ was used to sort the NK cells for expansion. We used NK MACS Medium (Miltenyi Biotec) with 5% human AB serum (Sigma-Aldrich) and 500 U/mL Interleukin 2 (IL-2) to culture the NK cells. 10 U/mL DNase I treatment is necessary to prevent cell aggregation and death after thawing. Afterward, we utilized the NK killing assay to measure the NK cytotoxicity. Briefly, NK cells were treated with IL-2 (500 U/mL) for expansion and stained with chMC81370-SCT-conjugated FITC and sorted by FACSARIAIIU (BD Biosciences). The sorted NK cells were resuspended in NK MACS medium system containing 500 U/mL IL-2 and then incubated at 37°C, 5% CO₂.

Analysis of the primary NK cells cytotoxicity via NK killing assay.

NK killing assay was performed using the LDH-GloTM Cytotoxicity Assay. The target cells (5,000 cells/100 μ L) were seeded into a 96-well flat-bottom microplate overnight. The RPMI Medium with 0.5% human AB serum and IL-2 (500 U/mL) was used as the NK

killing assay buffer. Then the effector cells (NK cells) in a 10:1 E/T ratio were added to the 96-well flat-bottom microplate, and the cells were incubated for additional 4 hours at 37°C, 5% CO₂. After incubation, the mixture was transferred to another 96-well microplate and 100x diluted by LDH storage buffer. The diluted mixture of 50 µL and LDH-detection buffer of 50 µL was mixed together. The microplate was incubated at room temperature of 1 hour, and the luminescence was read by the CLARIOstar. The data was calculated, and the statistical analyses were performed using GraphPad Prism software. The unpaired t test was used to test for statistical significance in NK killing assay. The percentage of target cells lysis was calculated according to the CDC assay formula: percentage of cell lysis = (luminescence of the experimental - luminescence of background)/(luminescence of the maximum - luminescence of background) × 100.

Supplementary Material

Refer to Web version on PubMed Central for supplementary material.

ACKNOWLEDGEMENT

We are grateful for all the materials and assistance from M. Hsiao (GRC, Academia Sinica). We thank Glycan Sequencing Core at GRC, Academia Sinica for the glycoform profiling. We also thank the Core Facilities of Translational Medicine of BioTRC (National Biotechnology Research Park, Academic Sinica) for the fluorescence imaging and data analysis. This research was supported by Academia Sinica Summit Program, NIH (AI-130227) and NSF (CHE-1954031).

References

1. Krasnova L, and Wong CH (2019) Oligosaccharide Synthesis and Translational Innovation, *J. Am. Chem. Soc.* 141, 3735–3754. [PubMed: 30716271]
2. Schnaar RL, Suzuki A, and Stanley P (2009) Glycosphingolipids, In *Essentials of Glycobiology*. 2nd edition, Cold Spring Harbor Laboratory Press.
3. D'Angelo G, Capasso S, Sticco L, and Russo D (2013) Glycosphingolipids: synthesis and functions, *FEBS J* 280, 6338–6353. [PubMed: 24165035]
4. D'Angelo G, Uemura T, Chuang C-C, Polishchuk E, Santoro M, Ohvo-Rekilä H, Sato T, Di Tullio G, Varriale A, and D'Auria S (2013) Vesicular and non-vesicular transport feed distinct glycosylation pathways in the Golgi, *Nature* 501, 116. [PubMed: 23913272]
5. Kojima N, and Hakomori S. i. (1991) Synergistic effect of two cell recognition systems: glycosphingolipid-glycosphingolipid interaction and integrin receptor interaction with pericellular matrix protein, *Glycobiology* 1, 623–630. [PubMed: 1822242]
6. Huang X, Schurman N, Handa K, and Hakomori S (2017) Functional role of glycosphingolipids in contact inhibition of growth in a human mammary epithelial cell line, *FEBS Lett* 591, 1918–1928. [PubMed: 28586101]
7. Iwabuchi K, Nakayama H, Oizumi A, Suga Y, Ogawa H, and Takamori K (2015) Role of ceramide from glycosphingolipids and its metabolites in immunological and inflammatory responses in humans, *Mediators of Inflammation* 2015.
8. Nakayama H, Yoshizaki F, Prinetti A, Sonnino S, Mauri L, Takamori K, Ogawa H, and Iwabuchi K (2008) Lyn-coupled LacCer-enriched lipid rafts are required for CD11b/CD18-mediated neutrophil phagocytosis of nonopsonized microorganisms, *J. Leuko. Biol* 83, 728–741. [PubMed: 18055569]
9. Karlsson K-A (1986) Animal glycolipids as attachment sites for microbes, *Chem. Phys. Lip* 42, 153–172.
10. Kakio A, Nishimoto S, Yanagisawa K, Kozutsumi Y, and Matsuzaki K (2002) Interactions of amyloid beta-protein with various gangliosides in raft-like membranes: importance of GM1

- ganglioside-bound form as an endogenous seed for Alzheimer amyloid, *Biochemistry* 41, 7385–7390. [PubMed: 12044171]
11. Ikeda K, Yamaguchi T, Fukunaga S, Hoshino M, and Matsuzaki K (2011) Mechanism of amyloid beta-protein aggregation mediated by GM1 ganglioside clusters, *Biochemistry* 50, 6433–6440. [PubMed: 21682276]
 12. Yagi-Utsumi M, Matsuo K, Yanagisawa K, Gekko K, and Kato K (2010) Spectroscopic Characterization of Intermolecular Interaction of Amyloid beta Promoted on GM1 Micelles, *Int. J. Alzheimers Dis* 2011, 925073. [PubMed: 21318130]
 13. Wu G, Lu ZH, Kulkarni N, and Ledeen RW (2012) Deficiency of ganglioside GM1 correlates with Parkinson's disease in mice and humans, *J. Neurosci. Res* 90, 1997–2008. [PubMed: 22714832]
 14. Gizaw ST, Koda T, Amano M, Kamimura K, Ohashi T, Hinou H, and Nishimura S (2015) A comprehensive glycome profiling of Huntington's disease transgenic mice, *Biochim. Biophys. Acta* 1850, 1704–1718. [PubMed: 25907331]
 15. Suzuki M, and Cheung NK (2015) Disialoganglioside GD2 as a therapeutic target for human diseases, *Expert. Opin. Ther. Targets* 19, 349–362. [PubMed: 25604432]
 16. Liu J, Zheng X, Pang X, Li L, Wang J, Yang C, and Du G (2018) Ganglioside GD3 synthase (GD3S), a novel cancer drug target, *Acta. Pharm. Sin. B* 8, 713–720. [PubMed: 30245960]
 17. Chang WW, Lee CH, Lee P, Lin J, Hsu CW, Hung JT, Lin JJ, Yu JC, Shao LE, Yu J, Wong C-H, and Yu AL (2008) Expression of Globo H and SSEA3 in breast cancer stem cells and the involvement of fucosyl transferases 1 and 2 in Globo H synthesis, *Proc. Natl. Acad. Sci. U. S. A* 105, 11667–11672. [PubMed: 18685093]
 18. Rahman MS, Spitzhorn LS, Wruck W, Hagenbeck C, Balan P, Graffmann N, Bohndorf M, Ncube A, Guillot PV, Fehm T, and Adjaye J (2018) The presence of human mesenchymal stem cells of renal origin in amniotic fluid increases with gestational time, *Stem. Cell. Res. Ther* 9, 113. [PubMed: 29695308]
 19. Harichandan A, Sivasubramaniyan K, Hennenlotter J, Schwentner C, Stenzl A, and Buhning HJ (2013) Isolation of adult human spermatogonial progenitors using novel markers, *J. Mol. Cell. Biol* 5, 351–353. [PubMed: 23929715]
 20. Virant-Klun I, Skutella T, Hren M, Gruden K, Cvjeticanin B, Vogler A, and Sinkovec J (2013) Isolation of small SSEA-4-positive putative stem cells from the ovarian surface epithelium of adult human ovaries by two different methods, *Biomed. Res. Int* 2013, 690415. [PubMed: 23509763]
 21. Huang YL, Hung JT, Cheung SK, Lee HY, Chu KC, Li ST, Lin YC, Ren CT, Cheng TJ, Hsu TL, Yu AL, Wu CY, and Wong CH (2013) Carbohydrate-based vaccines with a glycolipid adjuvant for breast cancer, *Proc. Natl. Acad. Sci. U. S. A* 110, 2517–2522. [PubMed: 23355685]
 22. Gottschling S, Jensen K, Warth A, Herth FJ, Thomas M, Schnabel PA, and Herpel E (2013) Stage-specific embryonic antigen-4 is expressed in basaloid lung cancer and associated with poor prognosis, *Eur. Respir. J* 41, 656–663. [PubMed: 22743677]
 23. Zhang W, Ding ML, Zhang JN, Qiu JR, Shen YH, Ding XY, Deng LF, Zhang WB, and Zhu J (2015) mTORC1 maintains the tumorigenicity of SSEA-4(+) high-grade osteosarcoma, *Sci. Rep* 5, 9604. [PubMed: 25853231]
 24. Nakamura Y, Miyata Y, Matsuo T, Shida Y, Hakariya T, Ohba K, Taima T, Ito A, Suda T, Hakomori SI, Saito S, and Sakai H (2019) Stage-specific embryonic antigen-4 is a histological marker reflecting the malignant behavior of prostate cancer, *Glycoconj. J* 36, 409–418. [PubMed: 31243630]
 25. Virant-Klun I, Kenda-Suster N, and Smrkolj S (2016) Small putative NANOG, SOX2, and SSEA-4-positive stem cells resembling very small embryonic-like stem cells in sections of ovarian tissue in patients with ovarian cancer, *J. Ovarian Res* 9, 12. [PubMed: 26940129]
 26. Noto Z, Yoshida T, Okabe M, Koike C, Fathy M, Tsuno H, Tomihara K, Arai N, Noguchi M, and Nikaido T (2013) CD44 and SSEA-4 positive cells in an oral cancer cell line HSC-4 possess cancer stem-like cell characteristics, *Oral. Oncol* 49, 787–795. [PubMed: 23768762]
 27. Sivasubramaniyan K, Harichandan A, Schilbach K, Mack AF, Bedke J, Stenzl A, Kanz L, Niederfellner G, and Buhning HJ (2015) Expression of stage-specific embryonic antigen-4 (SSEA-4) defines spontaneous loss of epithelial phenotype in human solid tumor cells, *Glycobiology* 25, 902–917. [PubMed: 25978997]

28. Aloia A, Petrova E, Tomiuk S, Bissels U, Deas O, Saini M, Zickgraf FM, Wagner S, Spaich S, Sutterlin M, Schneeweiss A, Reitberger M, Ruberg S, Gerstmayer B, Agorku D, Knobel S, Terranegra A, Falleni M, Soldati L, Sprick MR, Trumpp A, Judde JG, Bosio A, Cairo S, and Hardt O (2015) The sialyl-glycolipid stage-specific embryonic antigen 4 marks a subpopulation of chemotherapy-resistant breast cancer cells with mesenchymal features, *Breast. Cancer Res* 17, 146. [PubMed: 26607327]
29. Zhang S, Cordon-Cardo C, Zhang HS, Reuter VE, Adluri S, Hamilton WB, Lloyd KO, and Livingston PO (1997) Selection of tumor antigens as targets for immune attack using immunohistochemistry: I. Focus on gangliosides, *Int. J. Cancer* 73, 42–49. [PubMed: 9334808]
30. Wang CC, Huang YL, Ren CT, Lin CW, Hung JT, Yu JC, Yu AL, Wu CY, and Wong C-H (2008) Glycan microarray of Globo H and related structures for quantitative analysis of breast cancer, *Proc. Natl. Acad. Sci. U. S. A* 105, 11661–11666. [PubMed: 18689688]
31. Danishefsky SJ, Shue YK, Chang MN, and Wong CH (2015) Development of Globo-H cancer vaccine, *Acc. Chem. Res* 48, 643–652. [PubMed: 25665650]
32. Lou YW, Wang PY, Yeh SC, Chuang PK, Li ST, Wu CY, Khoo KH, Hsiao M, Hsu TL, and Wong C-H (2014) Stage-specific embryonic antigen-4 as a potential therapeutic target in glioblastoma multiforme and other cancers, *Proc. Natl. Acad. Sci. U.S.A* 111, 2482–2487. [PubMed: 24550271]
33. Cheung SK, Chuang PK, Huang HW, Hwang-Verslues WW, Cho CH, Yang WB, Shen CN, Hsiao M, Hsu TL, Chang CF, and Wong C-H (2016) Stage-specific embryonic antigen-3 (SSEA-3) and beta3GalT5 are cancer specific and significant markers for breast cancer stem cells, *Proc. Natl. Acad. Sci. U. S. A* 113, 960–965. [PubMed: 26677875]
34. Chuang PK, Hsiao M, Hsu TL, Chang CF, Wu CY, Chen BR, Huang HW, Liao KS, Chen CC, Chen CL, Yang SM, Kuo CW, Chen P, Chiu PT, Chen IJ, Lai JS, Yu CT, and Wong C-H (2019) Signaling pathway of globo-series glycosphingolipids and beta1,3-galactosyltransferase V (beta3GalT5) in breast cancer, *Proc. Natl. Acad. Sci. U. S. A* 116, 3518–3523. [PubMed: 30808745]
35. Lin CW, Tsai MH, Li ST, Tsai TI, Chu KC, Liu YC, Lai MY, Wu CY, Tseng YC, Shivatara SS, Wang CH, Chao P, Wang SY, Shih HW, Zeng YF, You TH, Liao JY, Tu YC, Lin YS, Chuang HY, Chen CL, Tsai CS, Huang CC, Lin NH, Ma C, Wu CY, and Wong C-H (2015) A common glycan structure on immunoglobulin G for enhancement of effector functions, *Proc. Natl. Acad. Sci. U. S. A* 112, 10611–10616. [PubMed: 26253764]
36. Seo Y, Ishii Y, Ochiai H, Fukuda K, Akimoto S, Hayashida T, Okabayashi K, Tsuruta M, Hasegawa H, and Kitagawa Y (2014) Cetuximab-mediated ADCC activity is correlated with the cell surface expression level of EGFR but not with the KRAS/BRAF mutational status in colorectal cancer, *Oncol. Rep* 31, 2115–2122. [PubMed: 24626880]
37. Velders MP, van Rhijn CM, Oskam E, Fleuren GJ, Warnaar SO, and Litvinov SV (1998) The impact of antigen density and antibody affinity on antibody-dependent cellular cytotoxicity: relevance for immunotherapy of carcinomas, *Br. J. Cancer* 78, 478–483. [PubMed: 9716030]
38. Jandus C, Boligan KF, Chijioko O, Liu H, Dahlhaus M, Demoulins T, Schneider C, Wehrli M, Hunger RE, Baerlocher GM, Simon HU, Romero P, Munz C, and von Gunten S (2014) Interactions between Siglec-7/9 receptors and ligands influence NK cell-dependent tumor immunosurveillance, *J. Clin. Invest* 124, 1810–1820. [PubMed: 24569453]
39. Kent SP, Ryan KH, and Siegel AL (1978) Steric hindrance as a factor in the reaction of labeled antibody with cell surface antigenic determinants, *J. Histochem. Cytochem* 26, 618–621. [PubMed: 357645]
40. De Vita M, Catzola V, Buzzonetti A, Fossati M, Battaglia A, Zamai L, and Fattorossi A (2015) Unexpected interference in cell surface staining by monoclonal antibodies to unrelated antigens, *Cytometry B. Clin. Cytom* 88, 352–354. [PubMed: 25327621]
41. Lu LL, Suscovich TJ, Fortune SM, and Alter G (2018) Beyond binding: antibody effector functions in infectious diseases, *Nat. Rev. Immunol* 18, 46–61. [PubMed: 29063907]
42. Bryceson YT, March ME, Ljunggren HG, and Long EO (2006) Synergy among receptors on resting NK cells for the activation of natural cytotoxicity and cytokine secretion, *Blood* 107, 159–166. [PubMed: 16150947]

43. Bhatnagar N, Ahmad F, Hong HS, Eberhard J, Lu IN, Ballmaier M, Schmidt RE, Jacobs R, and Meyer-Olson D (2014) Fcγ₃ (CD16)-mediated ADCC by NK cells is regulated by monocytes and Fcγ₂ (CD32), *Eur. J. Immunol* 44, 3368–3379. [PubMed: 25100508]
44. Lopez E, Scott NE, Wines BD, Hogarth PM, Wheatley AK, Kent SJ, and Chung AW (2019) Low pH Exposure During Immunoglobulin G Purification Methods Results in Aggregates That Avidly Bind Fcγ Receptors: Implications for Measuring Fc Dependent Antibody Functions, *Front. Immunol* 10, 2415. [PubMed: 31681303]
45. Geuijen KPM, Oppers-Tiemen C, Egging DF, Simons PJ, Boon L, Schasfoort RBM, and Eppink MHM (2017) Rapid screening of IgG quality attributes - effects on Fc receptor binding, *FEBS Open Bio* 7, 1557–1574.
46. Shah DD, Zhang J, Hsieh MC, Sundaram S, Maity H, and Mallela KMG (2018) Effect of Peroxide- Versus Alkoxy-Induced Chemical Oxidation on the Structure, Stability, Aggregation, and Function of a Therapeutic Monoclonal Antibody, *J. Pharm. Sci* 107, 2789–2803. [PubMed: 30075161]
47. Shah DD, Zhang J, Maity H, and Mallela KMG (2018) Effect of photo-degradation on the structure, stability, aggregation, and function of an IgG1 monoclonal antibody, *Int. J. Pharm* 547, 438–449. [PubMed: 29883793]
48. Aceto N, Bardia A, Miyamoto DT, Donaldson MC, Wittner BS, Spencer JA, Yu M, Pely A, Engstrom A, Zhu H, Brannigan BW, Kapur R, Stott SL, Shioda T, Ramaswamy S, Ting DT, Lin CP, Toner M, Haber DA, and Maheswaran S (2014) Circulating tumor cell clusters are oligoclonal precursors of breast cancer metastasis, *Cell* 158, 1110–1122. [PubMed: 25171411]
49. Bidard FC, Vincent-Salomon A, Sigal-Zafrani B, Dieras V, Mathiot C, Mignot L, Thiery JP, Sastre-Garau X, and Pierga JY (2008) Prognosis of women with stage IV breast cancer depends on detection of circulating tumor cells rather than disseminated tumor cells, *Ann. Oncol* 19, 496–500. [PubMed: 18187488]
50. Riethdorf S, Muller V, Zhang L, Rau T, Loibl S, Komor M, Roller M, Huober J, Fehm T, Schrader I, Hilfrich J, Holms F, Tesch H, Eidtmann H, Untch M, von Minckwitz G, and Pantel K (2010) Detection and HER2 expression of circulating tumor cells: prospective monitoring in breast cancer patients treated in the neoadjuvant GeparQuattro trial, *Clin. Cancer Res* 16, 2634–2645. [PubMed: 20406831]
51. Wang G, Benasutti H, Jones JF, Shi G, Benchimol M, Pingle S, Kesari S, Yeh Y, Hsieh LE, Liu YT, Elias A, and Simberg D (2018) Isolation of Breast cancer CTCs with multitargeted buoyant immunomicrobubbles, *Colloids Surf B Biointerfaces* 161, 200–209. [PubMed: 29080504]
52. Loeian MS, Mehdi Aghaei S, Farhadi F, Rai V, Yang HW, Johnson MD, Aqil F, Mandadi M, Rai SN, and Panchapakesan B (2019) Liquid biopsy using the nanotube-CTC-chip: capture of invasive CTCs with high purity using preferential adherence in breast cancer patients, *Lab Chip* 19, 1899–1915. [PubMed: 31049504]

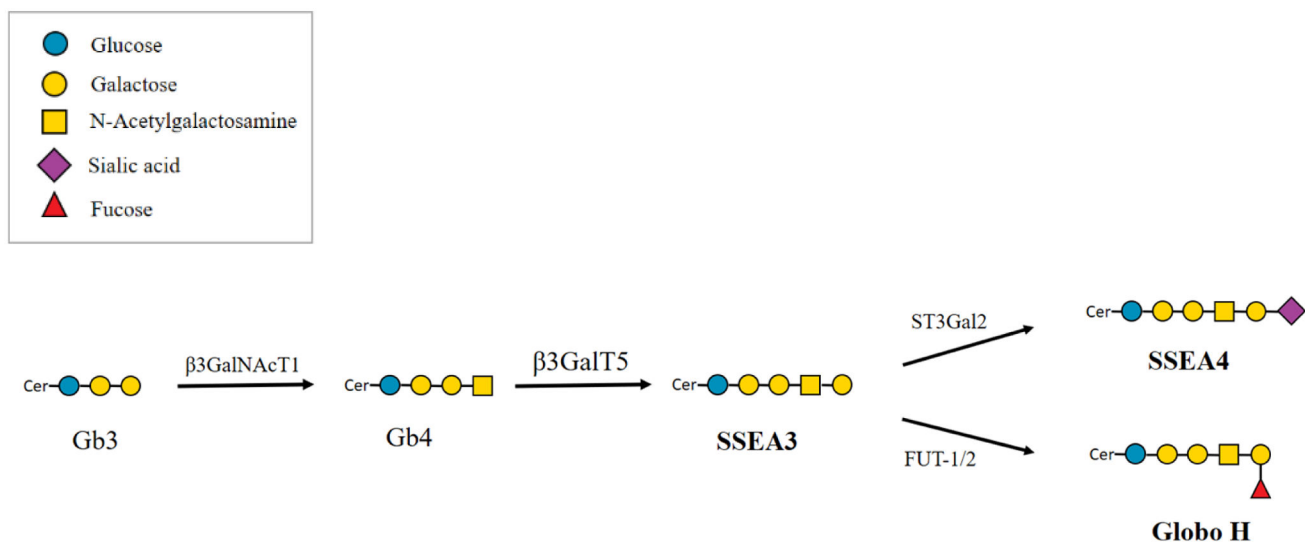


Figure 1. Biosynthesis of globo-series glycosphingolipids. Gb3, globotriaose; Gb4, globotetraose; SSEA3, stage-specific embryonic antigen 3; SSEA4, stage-specific embryonic antigen 4; β 3GalNAcT1, β 1,3-N-acetylgalactosaminyltransferase 1; β 3GalT5, β 1,3-galactosyltransferase V; ST3Gal-II, β -galactoside α 2,3-sialyltransferase; FUT-1, fucosyltransferase-1; FUT-2, fucosyltransferase-2.

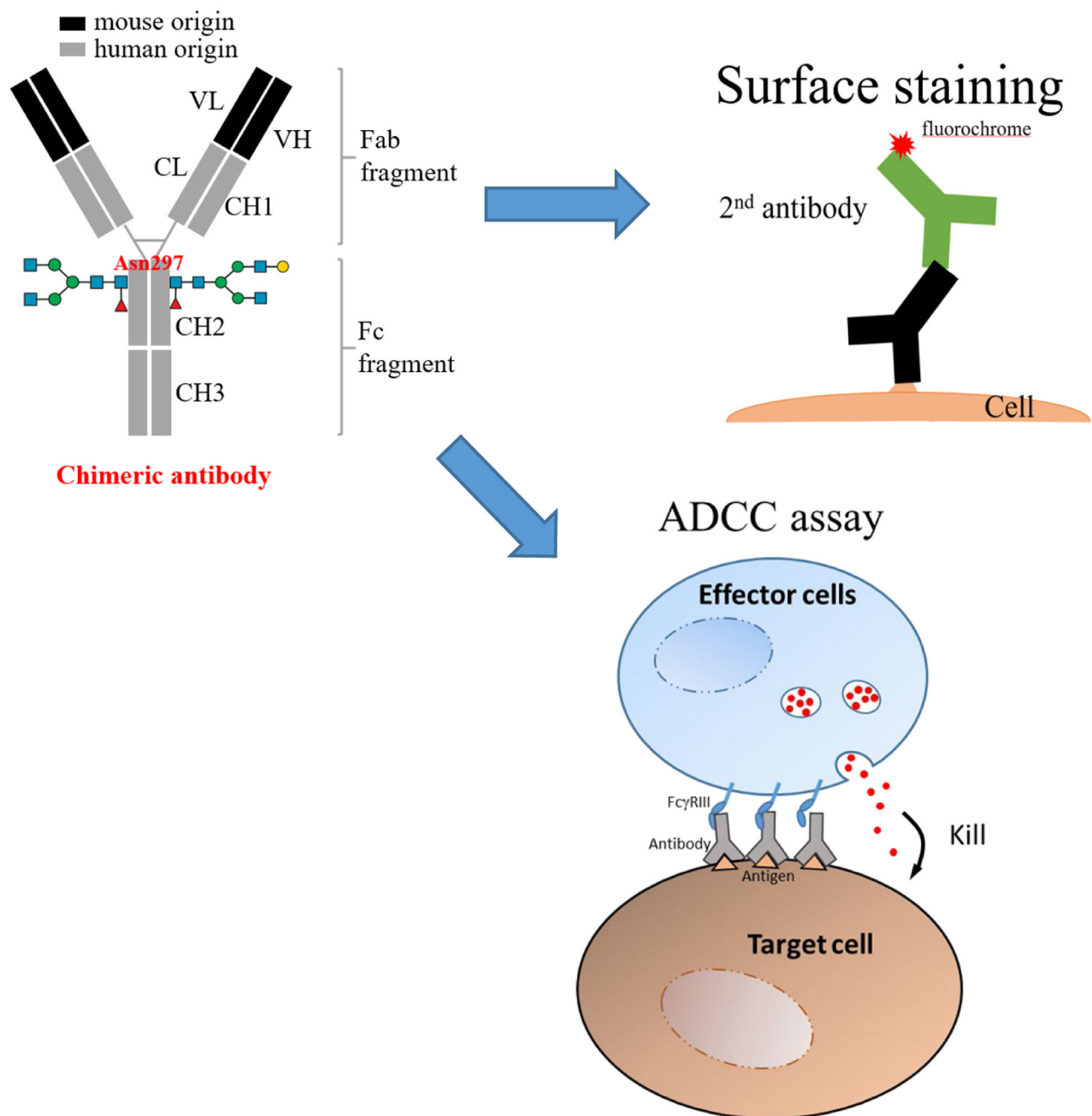


Figure 2.

A schematic presentation of research approach. To understand whether synergistic effect 34 can be reproduced *in vitro*, we evaluated the combined effect of anti-SSEA4 and anti-Globo H antibodies by ADCC assay, and performed staining to detect the surface expression level of SSEA4 and Globo H as a reference. For surface staining, chimeric or mouse (not shown) antibodies were used. Antibody labeling for detection could be direct (not shown) or indirect. For ADCC assay, only chimeric antibodies were used.

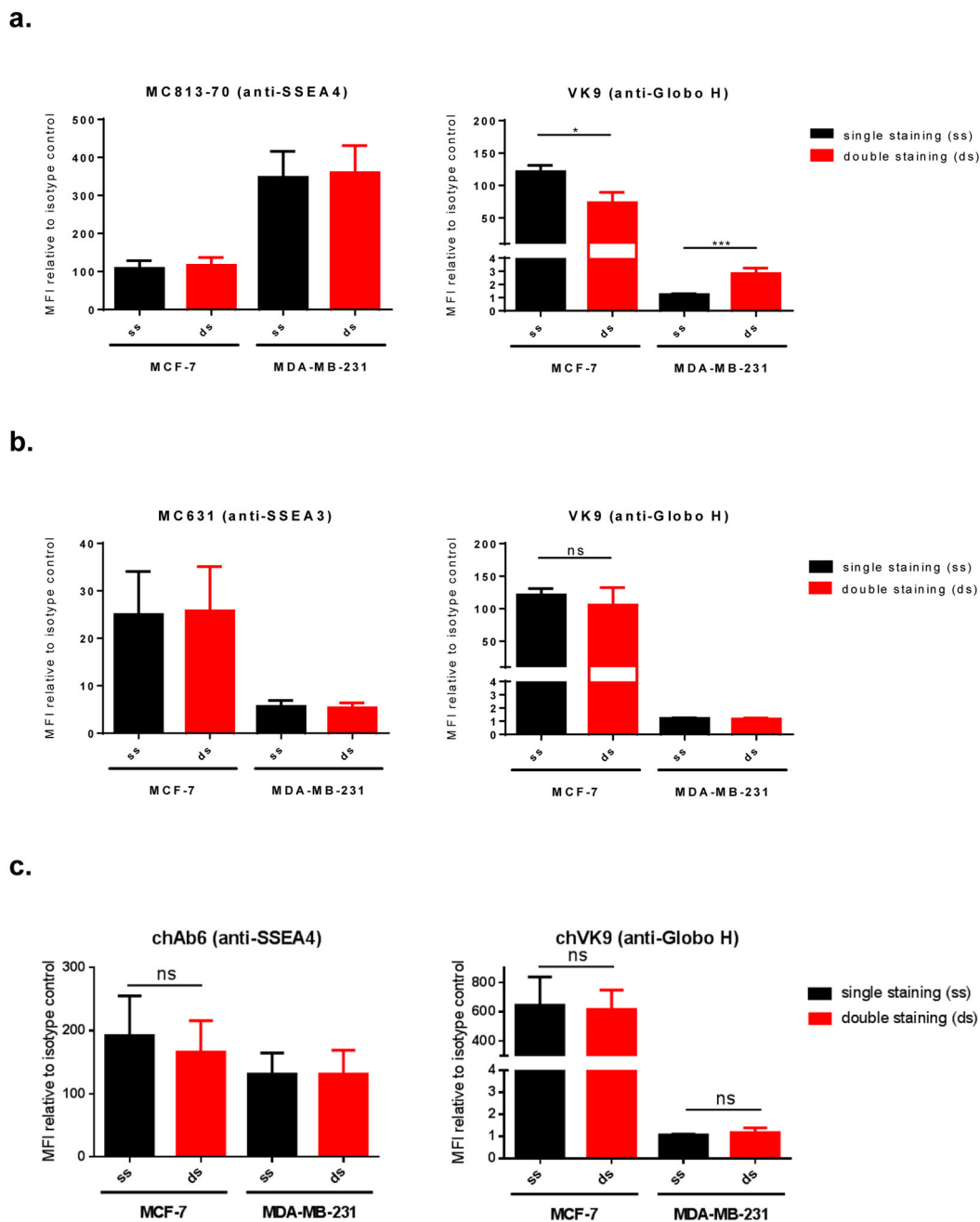


Figure 3.

Surface staining of globo-series GSLs on MCF-7 and MDA-MB-231. **a.** Double staining of SSEA4 and Globo H using AF488-conjugated MC813-70 and APC-conjugated VK9 (mouse antibodies). VK9 signal difference was observed: MCF-7 showed reduced double staining signal, while MDA-MB-231 showed increased double staining signal. This indicates that VK9 does not affect antigen binding of MC813-70, but MC813-70 affects antigen binding of VK9. The scatter plots are provided in Figure S1. **b.** Double staining of SSEA3 and Globo H using AF488-conjugated MC631 and APC-conjugated VK9 (mouse antibodies). Single staining and double staining signals were similar for both MC631 and

VK9, indicating the two antibodies do not affect each other when binding antigens. **c**, Double staining of SSEA4 and Globo H using FITC-conjugated chAb6 and APC-conjugated chVK9 antibodies. Single staining and double staining signals were similar for both chAb6 and chVK9, indicating the two antibodies do not affect each other when binding antigens. To determine whether the two antibodies influence each other when binding antigens, we compared the staining signals mean fluorescence intensities (MFIs, represent the geometric mean intensities) relative to isotype control between single staining (ss, in black) and double staining (ds, in red) in each cell line.

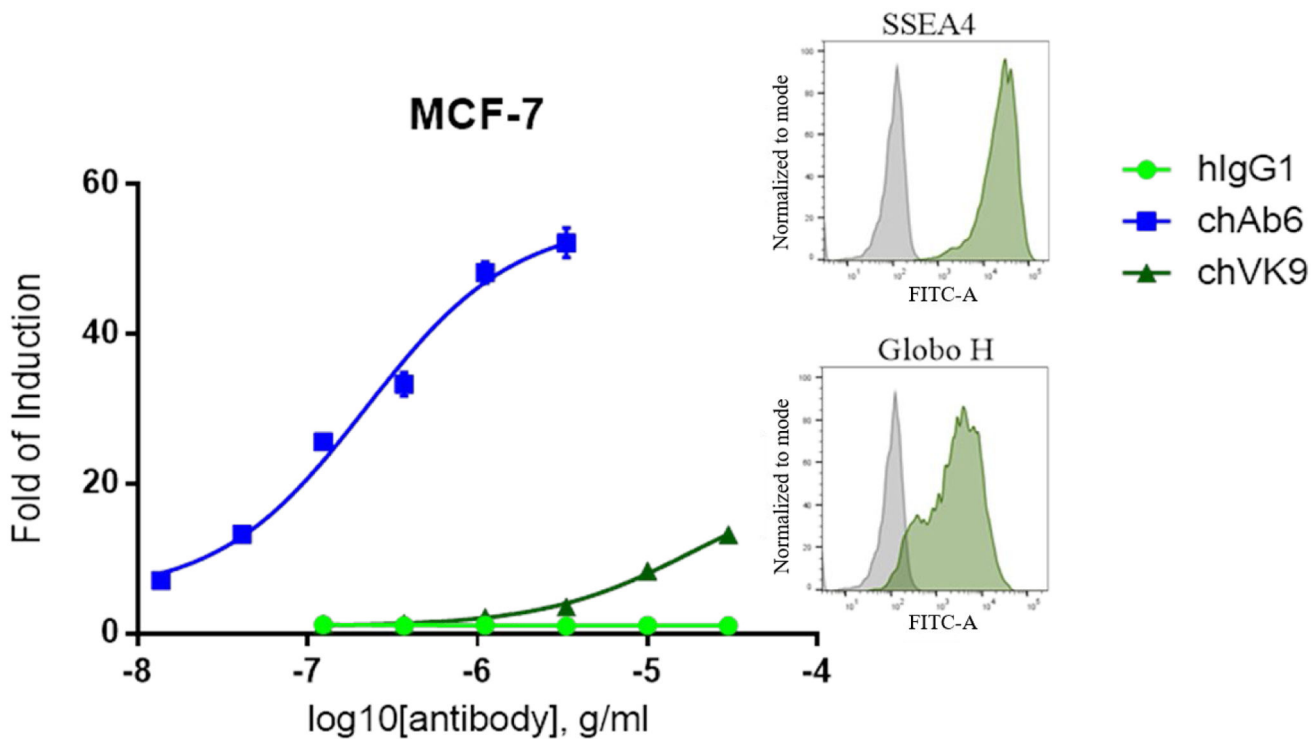


Figure 4. ADCC induction of chimeric Ab6 and chimeric VK9 and relative expression levels of SSEA4 and Globo H on MCF-7. ADCC assay was performed as described in Methods. The results showed that chAb6 induced stronger ADCC response than chVK9 due to high SSEA4 expression. Fold of induction is calculated as described in Methods. Surface staining was performed by indirect method using 10 μ g/ml unconjugated chAb6 or chVK9. The raw data are provided in Table S1.

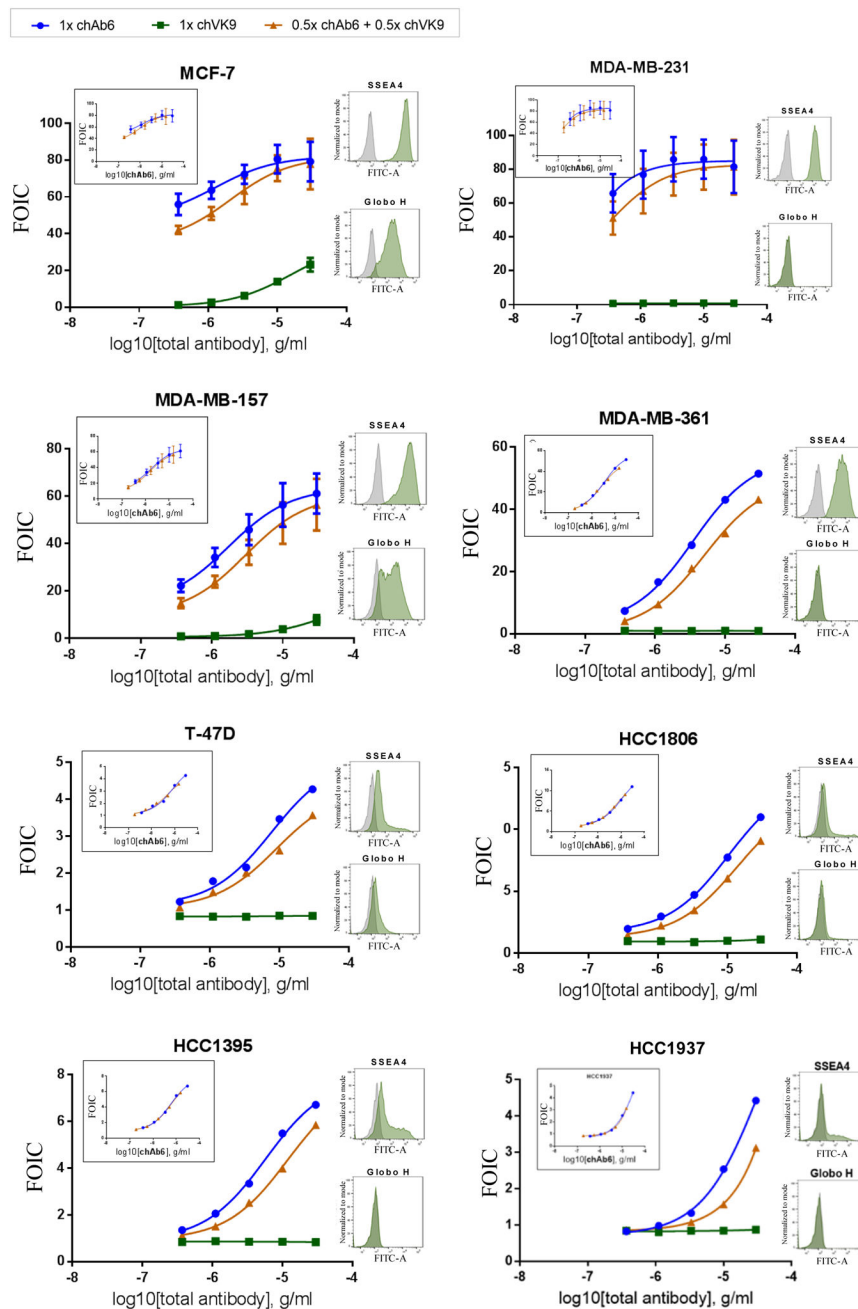


Figure 5. Combined effect of chAb6 and chVK9 in ADCC assay on various breast cancer cell lines. In combination, half the amount of each antibody was added. The results showed that chAb6 induced most of ADCC response in combination, whereas chVK9 induced very little. For y-axis, FOIC stands for fold of induction (test/calibrator): Fold of induction (calculated as described in Methods) is divided by a common calibrator, in which 0.183 ng/ml Rituximab and WIL2-S (target cell) were used to compare between different cell lines. In the main graphs, FOIC was plotted against total antibody concentration. The inset graphs were generated by changing x-axis to chAb6 concentration. Surface staining was performed by

indirect method using 10 $\mu\text{g/ml}$ unconjugated chAb6 or chVK9. The raw data are provided in Table S2.

Author Manuscript

Author Manuscript

Author Manuscript

Author Manuscript

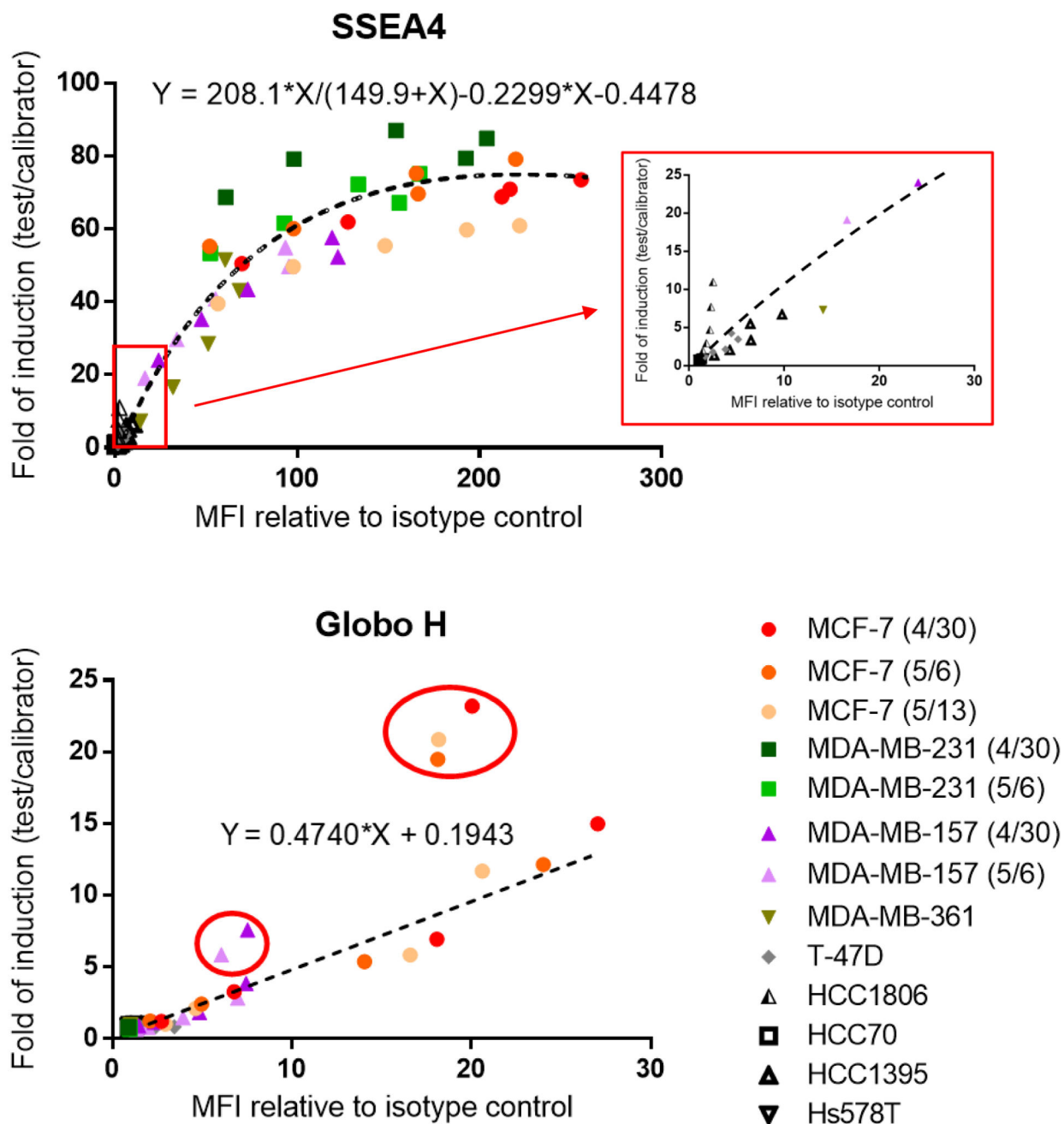


Figure 6.

Correlation of staining signal with ADCC response on various breast cancer cell lines. SSEA4 and Globo H showed positive correlation between staining signal and ADCC response. Surface staining was performed by indirect method. Each point correlates one MFI relative to isotype control with one-fold of induction for a single antibody concentration. Each symbol represents a breast cancer cell line, and different colors in each symbol represent independent experiments. A zoomed-in SSEA4 dot plot (in red box) is shown to compare with Globo H dot plot. Best-fit line or curve was generated using GraphPad Prism

6 software. Points circled in red are indicated as outliers of the best-fit line, and for these points 30 $\mu\text{g/ml}$ chVK9 was used. The raw data are provided in Table S3.

Author Manuscript

Author Manuscript

Author Manuscript

Author Manuscript

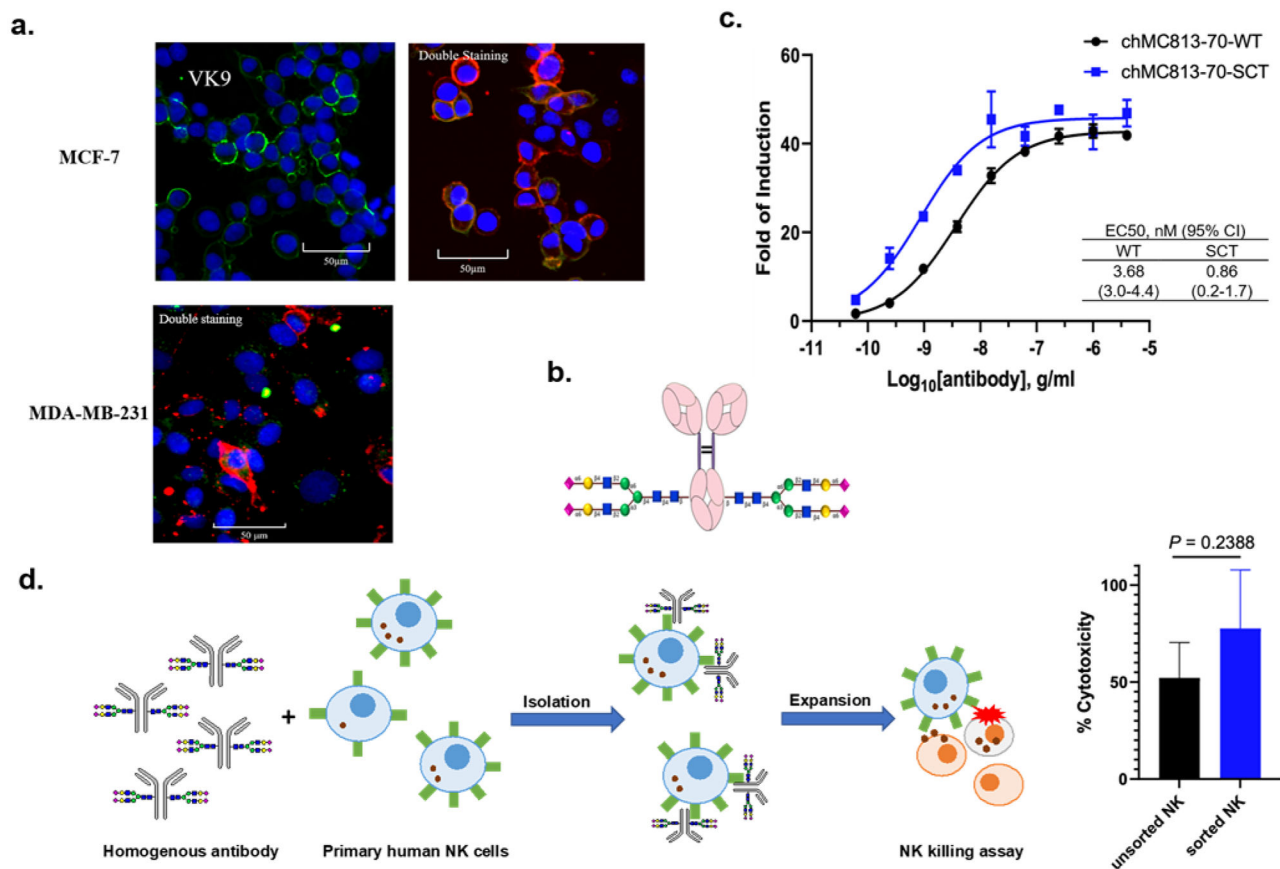








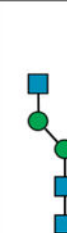


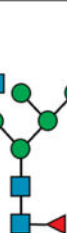
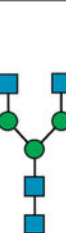
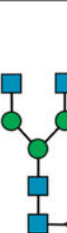












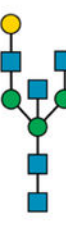

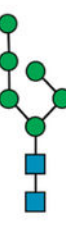


Figure 7.

a. Opera Phenix™ Image of MCF-7 and MDA-MB-231 breast cancer cells stained with FICT-conjugated VK9 (green, targeting Globo-H) only, or with the mixture of APC-conjugated MC813-70 (red, targeting SSEA4) and FICT-conjugated VK9 in a 1:50 ratio (0.5 μg/ml : 25 μg/ml). The results showed that cells are still predominantly interacting with MC813-70. At 1:1 ratio, the cancer cell is completely occupied by MC813-70. Nucleus is in blue (Hoechst 33342 (x 1/500)). **b.** Homogeneous antibody MC813-70-SCT with maximized ADCC activity for the isolation of NK cells enriched with FcγIIIa receptor responsible for the ADCC activity. **c.** Comparison of heterogeneous and homogeneous chMC813-70 in ADCC assay. The half-maximal effective concentrations (EC50) for chMC813-70-WT were 3.68 ng/mL against MDA-MB-231, and chMC813-70-SCT were 0.86 ng/mL against MDA-MB-231. **d.** Use of homogeneous antibody chMC813-70-SCT for isolation and expansion of a subpopulation of NK cells enriched with FcγIIa receptor which exhibited around 23% increase in killing the target cells (breast cancer cell line MDA-MB-231 with high expression of SSEA4).

Table 1.

N-glycan compositions of chimeric Ab6 and chimeric VK9. ChAb6 and chVK9 were first digested by trypsin to produce glycopeptides (described in Methods), and then were analyzed for glycoforms by mass spectrometry. Non-core fucosylated N-glycans are shown as exploded slices. Numbers indicate the percentages of total N-glycan.

| | | | | | | | | |
|--------|--|--|--|--|--|--|--|---|
| Symbol |  |  |  |  |  |  |  |  |
| Name | A1 | FA1 | FA1G1 | Hybrid | A2 | FA2 | A2G1 | FA2G1 |
| |  |  |  |  |  |  |  |  |
| Symbol |  |  |  |  |  |  | | |
| Name | A2G2 | FA2G2 | A2B | FA2B | A2BG1 | High mannose | | |
| | | | | | | H5N2 | H7N2 | |
| |  |  |  |  |  |  |  | |

